Pergamon

Int. J. Heat Mass Transfer. Vol. 38, No. 4, pp. 629–641, 1995

0017–9310/95 $9.50+0.00

0017–9310(94)00193–6

Effects of heater length and orientation on the trigger mechanism for near-saturated flow boiling critical heat flux—I. Photographic study and statistical characterization of the near-wall interfacial features

CHRISTOPHER O. GERSEY and ISSAM MUDAWAR†
Boiling and Two-Phase Flow Laboratory, School of Mechanical Engineering, Purdue University,
West Lafayette, IN 47907, U.S.A.

(*Received* 13 *December* 1993 *and in final form* 17 *June* 1994)

Abstract—Experiments were performed to explore the trigger mechanism for critical heat flux (CHF) on 10-, 30- and 110-mm long heaters which were mounted along one wall of a rectangular channel. The channel was oriented vertically, horizontally, and at an intermediate 45° angle with liquid FC-72 flowing above the heater surface. Using photomicrographic methods, still photographs and high speed video images were obtained normal to the heater surface through a transparent cover. The photographs revealed the formation of a wavy vapor layer on the heater prior to CHF with surface wetting occurring at the wave troughs. The vapor waves formed on the upstream portion of the heater and had wavelengths characteristic of the Kelvin–Helmholtz instability. The distance between wetting fronts increased in the stream-wise direction because of wave stretching and merging of adjacent waves. Eventually, midway down the long heater, the distance between the wetting fronts reached a constant asymptotic value. The overall impact of the stream-wise increase of wavelength was a reduction in the number of wetting fronts available for liquid replenishment of the heater surface causing a decrease in CHF with increasing heater length. Critical heat flux was triggered by lifting of the most upstream wetting front spurring a cessation of wetting front formation and a catastrophic cascading of wetting front lift off along the entire heater.

INTRODUCTION

Formulation of a theoretically-based CHF model requires knowledge and quantification of the physical mechanisms that initiate the CHF process. Determination of the trigger mechanism could potentially alleviate the need for massive new CHF data bases by eliminating the reliance on empirical correlations in favor of a physical model. Researchers typically rely on flow visualization to both formulate and confirm CHF models. Tong and Hewitt [1] critically reviewed the various CHF models using visual observations reported by several researchers to bolster as well as dispute the individual models.

Many researchers reported observing a large vapor patch in the vicinity of the boiling surface that restricted liquid replenishment of the surface [2–6]. In the sublayer dryout model, CHF was postulated to occur when a thin liquid film trapped between the vapor patch and the heater surface dried out. Fiori and Bergles [2] observed a large vapor patch to hover over their boiling surface trapping an approximately 0.06-mm sublayer of liquid. During the residence time of the patch, the liquid sublayer dried out, causing a momentary increase in the local wall temperature. Once the vapor patch detached, cool liquid rushed in and rewetted the surface; however, a new vapor bubble quickly formed and the process was repeated. They postulated CHF was triggered when the local wall temperature exceeded the Leidenfrost temperature, when liquid could no longer rewet the surface.

Hino and Ueda [7, 8] observed large vapor patches to travel over their heated surface in flow boiling. As CHF was approached, the residence time of vapor drastically increased, which greatly hindered liquid replenishment of the surface and increased the surface temperature. They also postulated CHF occurred when the sublayer dried out.

Recently, Galloway and Mudawar [9] clearly identified the trigger mechanism for CHF from a short heater in vertical upflow of FC-87 using photomicrography and high-speed video imaging of the near-wall region. At heat fluxes just below CHF (CHF−), bubbles emanating from the heater surface were observed to coalesce into a vapor wave adjacent to the surface. The wave traveled downstream, maintaining contact with the heater at the wave troughs. These moving contact regions amounted to wetting fronts over which the bulk flow could replenish the surface with liquid. While most of the heater surface was dry between wetting fronts, adequate cooling was possible because the heat could still be dissipated by

---

†Author to whom correspondence should be addressed.

NOMENCLATURE

b	fraction of wavelength occupied by the wetting front for waves with $\lambda = 2\lambda_c$
CHF	critical heat flux
CHF−	heat flux just below q''_m
CHF+	heat flux just above q''_m
g	gravitational acceleration
L	heater length (10, 30 or 110 mm)
L_1	span of heater corresponding to upstream doubling of wavelengths
L_2	span of heater where λ increases because of wave stretching and merging
L_3	span of heater where λ is constant
P	pressure
ΔP	pressure drop
q''	average wall heat flux
q''_m	critical heat flux
t	time
T	temperature
ΔT_{sub}	inlet subcooling, $T_{sat} - T_{f,in}$
U	mean velocity
z	stream-wise coordinate.

Greek symbols

λ	wavelength
λ_c	critical wavelength
σ	standard deviation
θ	orientation angle measured from the vertical position.

Subscripts

c	critical
f	liquid
in	inlet
meas	measured
sat	saturated
w	average wall condition.

intense boiling and evaporation at the wetting fronts. Galloway and Mudawar observed one to three wetting fronts were present on their 12.7-mm long heater depending on the flow conditions. Critical heat flux was triggered by lifting of the most upstream wetting front as a result of intense localized boiling in the upstream wetting front.

Unfortunately, the interfacial lift-off model proposed by Galloway and Mudawar was derived from observations and data obtained with only a short heater in vertical upflow. The question readily arises as to the validity of the model for longer heaters and orientations other than vertical upflow. The present paper is the first of a two-part investigation of near-wall vapor–liquid interactions and the CHF trigger mechanism on longer heaters in vertical, inclined, and horizontal flow. This study will determine if the interfacial lift-off CHF model proposed by Galloway and Mudawar can be extended to situations which are more representative of actual engineering systems. The most pertinent issue is the stream-wise development of vapor layer interfacial features and the propagation of wetting fronts on long heaters. Part II of this study [10] will detail the development of a CHF model for these conditions.

EXPERIMENTAL APPARATUS

Fluorinert FC-72 was circulated and conditioned to the desired inlet flow velocity, temperature, and pressure in the two-phase flow loop shown in Fig. 1(a), which is described in detail in ref. [11]. The test section, Fig. 1(b), has been used in several previous electronic cooling experiments [11–13] that featured an array of nine, discrete, in-line heat sources. This channel was modified in the present study to facilitate converging the flow from the inlet reservoir to the channel dimensions of 10 mm × 5 mm. Like the previous studies, the present also featured FC-72 as the working fluid because its relatively low boiling point and low CHF reduced the likelihood of catastrophic burnout of the channel and heater hardware. FC-72, a product of 3M Company, is an environmentally friendly, chlorine-free fluid derived from hydrocarbon compounds by replacing all of the hydrogen atoms bonded to carbon atoms with fluorine atoms.

Visual access normal to the heater surfaces was possible through a Lexan window facing the channel wall containing the flush-mounted heaters. Absolute and differential pressure measurements were made at the upstream and downstream edges of the respective heaters through ports in one of the channel side walls. Maintaining a slightly positive pressure in the condenser/reservoir prevented air leaks into the system. As a result, the nominal operating pressure at the upstream of the heater in operation was kept at 1.36 bar (20 psia) for all of the tests. The saturation temperature for FC-72 at this pressure is 66.18°C.

The channel could be rotated to one of three angles: 0° (vertical upflow), 45° (inclined flow) and 90° (horizontal flow). These angles provided a good coverage of the g-field effect on interfacial wave growth and CHF. The importance of orientation to the hydrodynamic instabilities associated with CHF will be discussed in Part II of the present study [10].

As shown in Fig. 1(b), the channel contained three heaters: short (10 mm), intermediate (30 mm) and long (110 mm). The most upstream edge of the 10-mm heater was 524.5 mm from the inlet reservoir. The 30- and 110-mm heaters were positioned downstream with a 10-mm space between heaters. Construction of the 10-, 30- and 110-mm heaters is illustrated in Fig.

2(a), (b) and (c), respectively. Each heater was machined from oxygen-free copper such that the heater surface in contact with the fluid measured 10 mm wide by 10, 30 or 110-mm long. The 10-mm heater was powered by a thick-film resistor which was silver soldered to the underside of the copper slab. Two thick-film resistors were soldered to the underside of the 30-mm heater and six resistors to the 110-mm heater. The surface temperature of the heater was inferred from thermocouples located just beneath the heater surface. The thermocouples were evenly spaced above and between each thick-film resistor; one thermocouple was located in the 10-mm heater, three in the 30-mm heater and eleven in the 110-mm heater. One-dimensional heat conduction was used to calculate the surface temperature above each of the thermocouples. A parallel electrical circuit powered the thick-film resistors. Variable resistors were installed in series with each thick-film resistor and adjusted so that each resistor dissipated the same power. One voltage transducer and up to six current transducers were used to calculate the power dissipation of each heater. The heat flux on the surfaces of the two longer heaters was calculated by dividing the total energy generated by all the resistors by the total heater surface area. In order to save the thick-film resistors from burnout, the data acquisition system was configured to shut off all electric power to the resistors once CHF had been reached. It should be stressed that *only one of the three heaters was operated during a given test*, so the heaters had no effect on one another.

A spray of water–particulate slurry, consisting of particles with an average size of 10 μm, was used to create a uniform surface texture on each heater prior to each set of experiments. Upon startup, the flow loop was deaerated for 20 min to remove non-condensible gases from the FC-72. The condensate

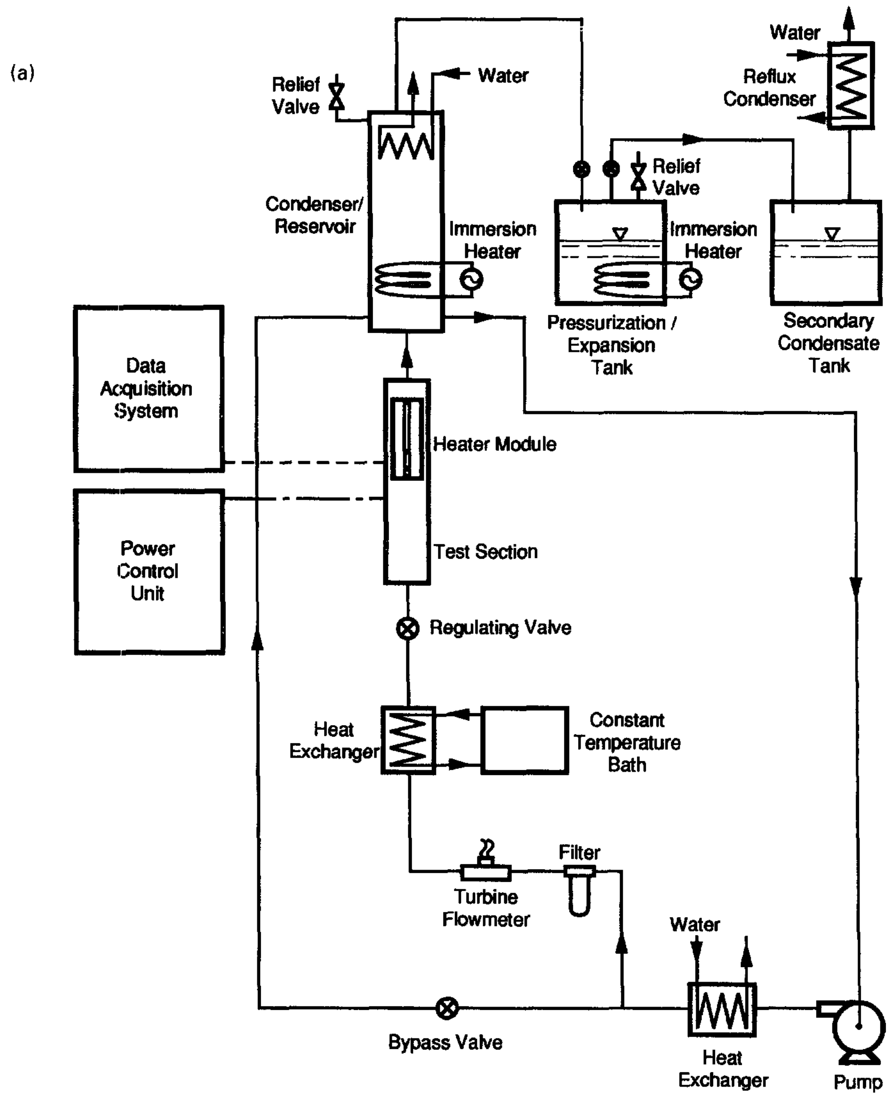

Fig. 1. Schematic of (a) flow loop and (b) test section.

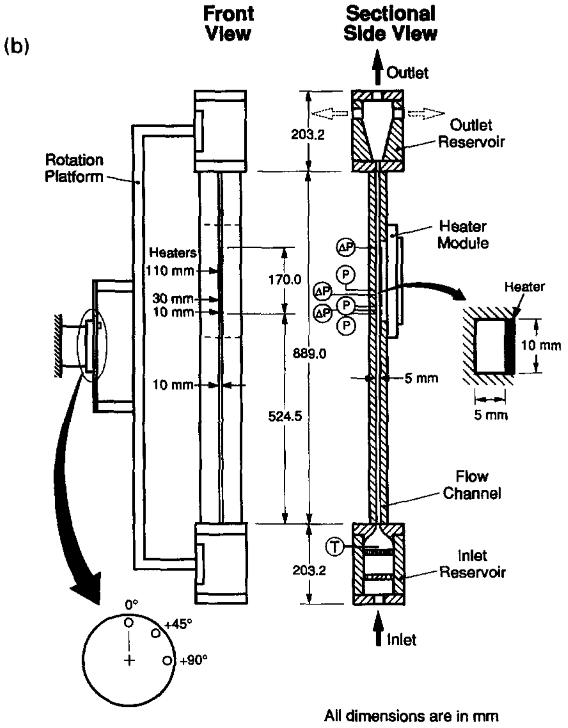

Fig. 1—*continued.*

tank captured the condensate returning from the reflux condenser while the noncondensible gases escaped to the atmosphere.

Although the focus of this study was to obtain CHF data, some single-phase and nucleate boiling data were also obtained. A data point was taken after the entire system attained steady-state. Steady-state was reached when each of the heater temperatures as well as the inlet reservoir temperature reached a standard deviation of less than 0.1°C over a period of 20 s. Near CHF, the heat flux increments were decreased to 0.5 W cm^{-2} to ensure that CHF was not reached prematurely. A large and rapid increase in the heater temperature always signaled the attainment of CHF. Critical heat flux was approximated as the last stable heat flux plus one half of the last power increment. Most of the CHF data were repeatable to $\pm 5\%$.

Propagation of error [14] was utilized in calculating some of the uncertainties associated with the experimental readings. Using information from the turbine flowmeter manufacturer, the maximum uncertainties in the velocity measurements were estimated to be $\pm 1.0\%$ for $U \leqslant 150$ cm s^{-1} and $\pm 2.68\%$ for $U > 150$ cm s^{-1}. The respective manufacturers of the pressure transducers estimated a $\pm 0.75\%$ uncertainty in the absolute pressure measurement and $\pm 1.0\%$ with the differential pressure transducer. All thermocouples were calibrated, and their maximum uncertainty was $\pm 3.6\%$ of absolute temperature reading. Lastly, maximum uncertainty in the heat flux measurements made by the voltage and current transducers was estimated to be $\pm 3.3\%$ at $q'' = 30$ W cm^{-2}. Heat losses from the heaters were minimized by constructing the heater substrate from G-7 fiberglass. A two-dimensional numerical analysis was performed on a cross-sectional slice of a 10-mm-wide heater; the largest heat loss was calculated to be 3%.

Still pictures and video images of the near-wall interfacial features were made with a 35-mm Nikon camera and a Kodak EktaPro 1000 video imager, the latter is capable of speeds up to 6000 partial frames per second. An array of standard lenses and close-up lens kits were utilized to maximize picture quality and resolution. Because the sides of the test section were constructed from opaque G-10 fiberglass, pictures could only be obtained in normal view through the Lexan window.

EXPERIMENTAL RESULTS

Visual observations of the vapor–liquid interface at CHF— were made for the 10-, 30- and 110-mm heaters, operated independently, at several inlet liquid velocities. The inlet velocity was varied from 25 to 200 cm s^{-1} at each of the three orientations while the inlet liquid temperature was held constant with $\Delta T_{sub} = 4$°C.

As the heat flux was increased, the 30- and 110-mm heaters sometimes displayed a gradual progression to fully developed nucleate boiling. In all of the tests, boiling incipience occurred on the most downstream portion of the respective heater first and then propagated upstream with increases in heat flux. Figure 3(a) and (b) shows the individual thermocouple readings

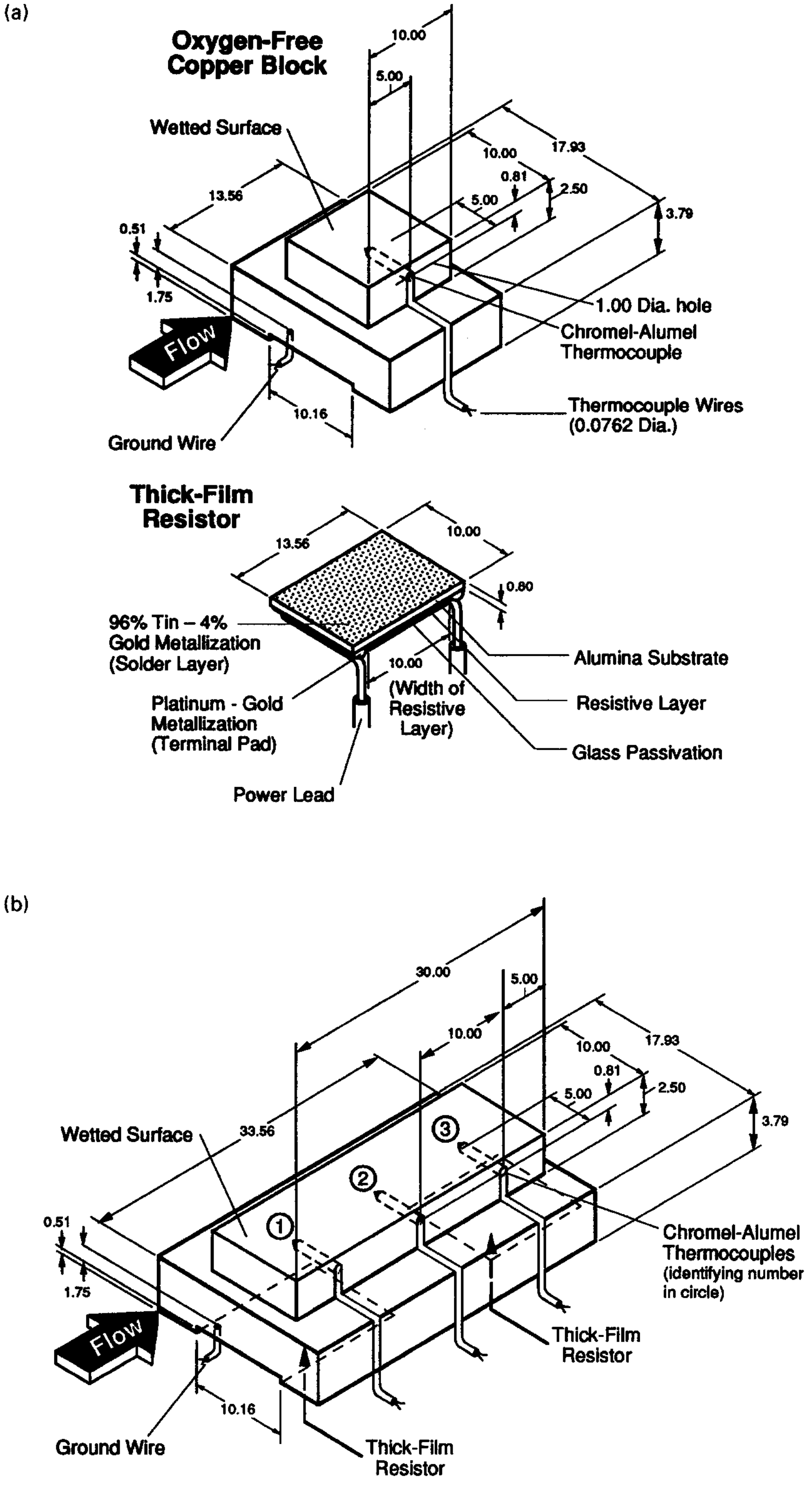

* All dimensions in mm.

Fig. 2. Construction of (a) 10-mm heater (with thick-film resistor), (b) 30-mm heater and (c) 110-mm heater.

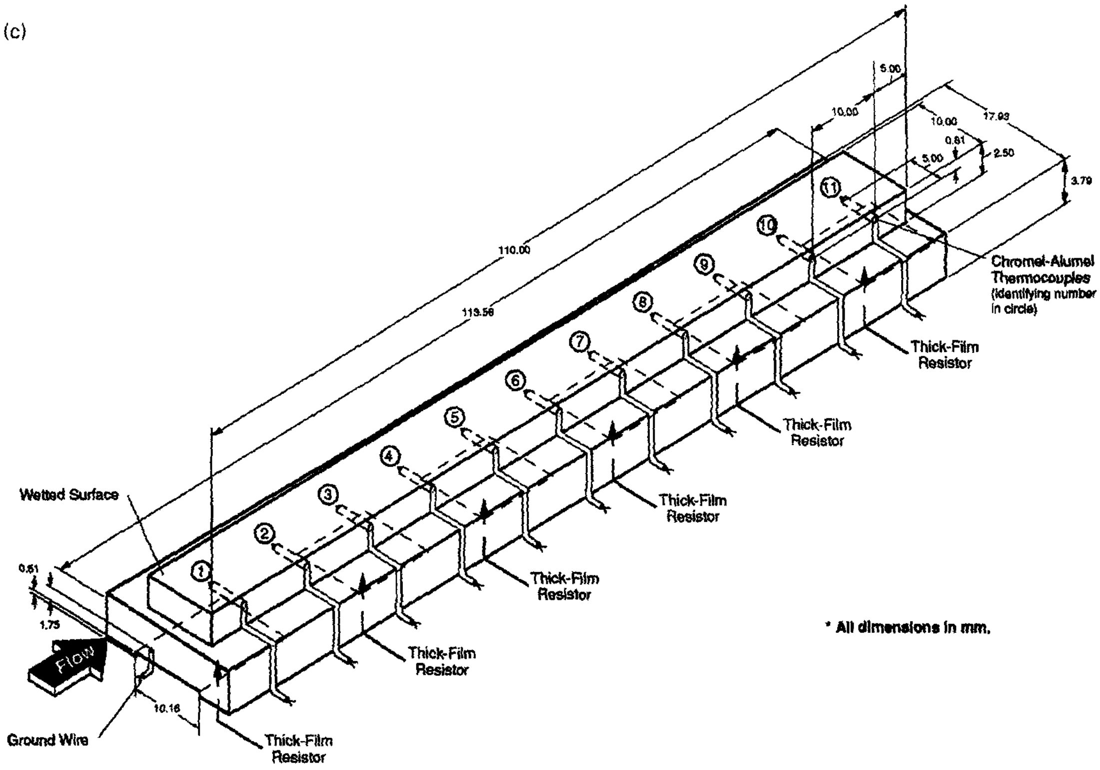

Fig. 2—*continued.*

plotted against the average wall heat flux for a few of the tests with the 30- and 110-mm heaters, respectively. This type of representation is employed instead of boiling curves because it highlights more effectively the stream-wise changes in surface temperature.

Figure 3(a) shows the effects of orientation on the three thermocouple readings of the 30-mm heater. Recall from Fig. 2(b) that thermocouple number 1 is the most upstream thermocouple, and number 3 is the most downstream thermocouple. At low heat fluxes, the entire heater surface was undergoing single-phase heat transfer, and the three temperatures increased with increasing heat flux. At the incipience of nucleate boiling, typically, the entire wall temperature would decrease. However, incipience on the long heaters was more gradual with nucleate boiling occurring over only the downstream portion of the heater. Increases in velocity typically delayed incipience on the upstream portion of each of the heaters to higher heat fluxes.

During partial nucleate boiling, heat could be routed from the upstream portion of the heater to the downstream portion where the heat transfer coefficient is higher. This rerouting of heat can explain the unique temperature behavior in the 30-mm heater, Fig. 3(a), for the 45° test. Initially, all three thermocouples read similar temperatures while the entire surface was in the single-phase regime. Nucleation commenced at $q'' = 5.5$ W cm^{-2}, but, because of the heat routing from upstream to downstream, all three thermocouple temperatures decreased simultaneously even though nucleation was visible only on the downstream portion of the heater. As the heat flux was increased, the temperature of the surface undergoing

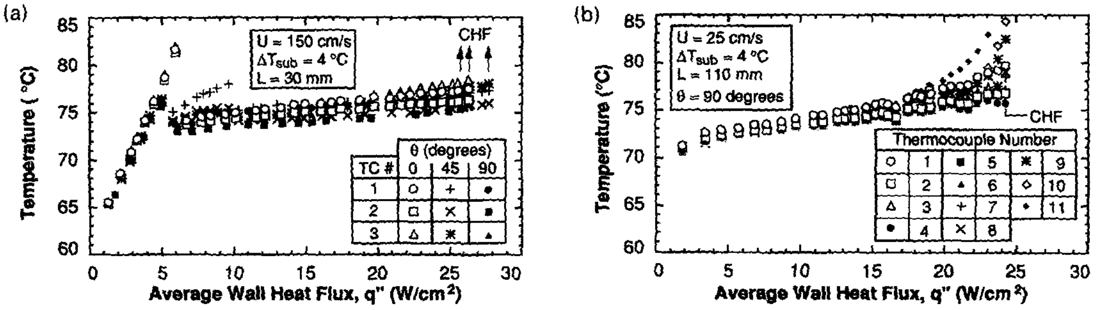

Fig. 3. Thermocouple temperatures illustrating effects of (a) orientation for the 30-mm heater and (b) stream-wise variations for the 110-mm heater.

single-phase heat transfer increased disproportionately relative to the rest of the surface because energy routing could not fully compensate for the stream-wise disparity in heat transfer coefficients. Figure 3(a) displays the stream-wise disparity in the thermocouple readings for $q'' = 5$–10 W cm^{-2} as well as the gradual convergence in the temperatures at higher heat fluxes. At CHF−, the entire heater surface was boiling except for a very small sliver at the most upstream edge of the heater. At these high heat fluxes, heat removal from the surface was accomplished at localized patches corresponding to wetting fronts in the vapor wave as described by Galloway and Mudawar [9]. The frequency of wetting fronts was sufficiently high to maintain a fairly uniform heat removal from the entire surface causing the thermocouple readings on the 30-mm heater to be relatively close to one another even at heat fluxes nearing CHF.

Figure 3(b) shows all 11 thermocouple readings for the 110-mm heater for the lowest velocity, 25 cm s^{-1}, and 90° (horizontal) orientation. Because of the low velocity, there was only a very small single-phase region, and the entire surface began boiling in unison at a very low heat flux. At higher liquid velocities, gradual incipience, similar to that observed on the 30-mm heater, occurred on the 110-mm heater. Uniformity in the nucleate boiling heat transfer coefficients in Fig. 3(a) and (b) may be inferred from the closeness of the temperature readings except near CHF. For many of the tests on the 110-mm heater, the downstream thermocouples exhibited measurable increases in temperature near CHF relative to the upstream thermocouples. As shown in Fig. 3(b), near CHF, thermocouples 9, 10 and 11 were all several degrees higher than the rest. This behavior is attributed to a decrease in the frequency of wetting front passage over the downstream portion of the heater as compared to the upstream portion. This phenomenon will be addressed in more detail in the next section.

For all three angles, CHF values at each inlet velocity were always highest on the 10-mm heater followed, in turn, by the 30- and 110-mm heaters. Figure 4(a)–(c) shows the CHF values obtained at the 0°, 45° and 90° orientations, respectively. Velocity can be seen to have a relatively minor effect on CHF throughout the data base. For a given liquid velocity, orientation also had no appreciable effect on CHF. Gersey and Mudawar [12, 13] found that changing the angle of orientation from 0 to 90° caused a slight decrease in CHF from nine, linearly-arranged, 10-mm long discrete heaters for velocities below 200 cm s^{-1}. Maddox and Mudawar [15] found that, for low inlet liquid velocities and near-saturated flow, the slope of the measured CHF vs velocity curve was indeed very small, $q''_m \propto U^{0.16}$.

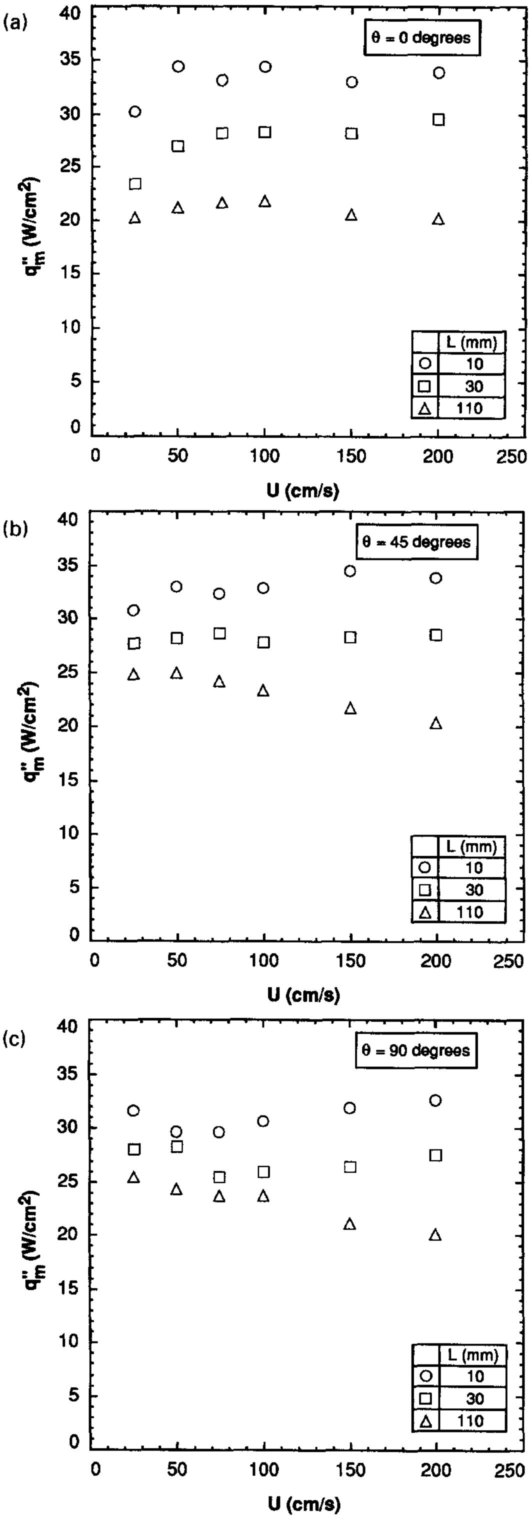

Fig. 4. Critical heat flux values for the three heaters at the (a) 0°, (b) 45° and (c) 90° orientations.

PHOTOGRAPHIC STUDY OF CHF

Vapor wave formation on the heater surface

CHF can only be modeled by observing conditions both at CHF− and CHF+. Attaining CHF+ ensures that the sequence of events corresponding to the previous heater power are representative of CHF−, and the transition between CHF− and CHF+ enables the detection of the CHF trigger mechanism. The ability to take both still pictures and video images is also crucial to depicting the CHF trigger mechanism. Still pictures produced high resolution images from which interfacial features could be measured and statistically analyzed, while video photography provided a sequential record of events which helped ascertain the relative importance of the depicted features to the CHF process.

Still pictures and video sequences captured normal to the heater surface at CHF– revealed the formation of a wavy vapor layer on the heated surface and provided a means to measure vapor wavelengths. Figure 5(a)–(c) shows photographs of CHF– conditions on the 10-, 30- and 110-mm heaters, respectively, at $U = 75$ cm s^{-1} in vertical upflow. The pictures were taken with a Nikon 35-mm camera fitted with a 200-mm lens and a 1/64 000 s, high-intensity flash. In order to obtain reasonable resolution on the 110-mm heater, only a third of the heater was photographed at a time; therefore, Fig. 5(c) is reconstructed from three different photographs. Wavelengths were measured on the series of photographs with the aid of a magnifying glass. Areas where the liquid–vapor interface made contact with the heater surface appear as dark regions; the distance between the centers of consecutive dark regions was recorded as the wavelength. The starting stream-wise position of the wave was also recorded, providing a means to quantify any stream-wise growth in the wavelength. Sample wavelengths are marked on their respective photographs [see Fig. 5(a)–(c)]; however, the mean values of wave features were determined from a statistical analysis of dozens of photographs and several minutes of video images. The major limitation to observing and measuring wavelengths from the normal view was the inability to observe the extent of surface wetting at each wetting front.

The wetting fronts (dark regions) in Fig. 5(a)–(c) seem fairly two-dimensional on each of the heaters. Typically, two to three wetting fronts existed on the 10-mm heater and five to six on the 30-mm heater. During the low velocity tests with the 110-mm heater, the downstream portion of the channel became blurred by the high void fraction. As the inlet liquid velocity was increased to about 75–100 cm s^{-1}, roughly 11–13 wetting fronts could be identified on the heater surface. The distances between wetting fronts on the first 10 mm of the 30- and 110-mm heaters, Fig 5(b) and (c), respectively, appear fairly equal to those on the 10-mm heater, Fig. 5(a). A stream-wise growth in the vapor wavelengths is evident on the two longer heaters.

Figure 6 shows the measured wavelengths from the three heaters in vertical upflow at $U = 100$ cm s^{-1}. Each wavelength is plotted with respect to the stream-wise position of its upstream edge. An exponential curve fit to the data is also shown. For all of the conditions tested, individual data for the 10-mm heater were scattered, but there appeared to be a tendency for wavelengths to increase along the heater. Wavelengths measured on the first 10 mm of the 30-mm heater fell within the scatter of wavelengths measured on the 10-mm heater. Similarly, wavelengths measured on the first 30 mm of the 110-mm heater overlapped wavelengths measured on both the 30-mm and 10-mm heaters, so there appears to be continuity in wave growth for the different heater lengths. On the latter part of the 110-mm heater, the waves still grew, but the wavelength leveled out as depicted in Figs. 5(c) and 6.

The growth and scatter of the measured wavelengths was investigated further by partitioning the heater into four stream-wise zones: 0–10 mm, 10–20 mm, 20–50 mm and 50–110 mm. The choice of these particular zones will become evident later. Wave measurements in each of the zones were grouped into bins of 1 mm (for instance, $0 < \lambda < 1$ mm and $1 < \lambda < 2$ mm). The percentage of the wave measurements in each bin was recorded for each of the four zones. Figure 7 shows these percentages at the centers of their respective bins for all of the vertical upflow tests. Changes in velocity had little effect on the measured wavelength for all of the tests. In their review article, Hewitt and Govan [16] report that, in some of his earlier work, Hewitt also observed wavelengths on an annular liquid film to be independent of phase flow rates. In the present study, the majority of the waves on the first 10 mm of the three heaters were centered around $\lambda_{meas} = 3$ mm. By $10 < z < 20$ mm, the waves had grown as well as spread out; most of the waves were between 5 and 10 mm. The next stream-wise zone, 20–50 mm, had larger wavelengths than the 10–20 mm zone. The final zone encompasses all of the measurements made after 50 mm on the 110-mm heater. This zone displayed both a continued broadening of the wavelength histogram and a constant asymptotic wavelength at $\lambda_{meas} = 10$–12 mm.

Using a 12.7-mm heater, Galloway and Mudawar [17] measured all of their wavelengths at two-thirds of the heater length. At this location, the average wavelength was found to be twice the critical wavelength, λ_c, determined by the Kelvin–Helmholtz instability; a small growth in the wavelength was observed along their heater. They observed that waves were generated on the upstream edge of the heater with a wavelength equal to λ_c. As a wetting front was formed by the approaching wave, severe boiling and evaporation prevented the next approaching wave from forming a wetting front. Thus, a wetting front was established with every other upstream wave and the resulting wetting fronts were separated by $2\lambda_c$. As shown in Fig. 7, the wavelengths measured on the first 10 mm of the three heaters in the present study were approximately equal to λ_c. Because the heaters could be observed only in normal view, it is possible that some of the wavelength measurements made on the first 10 mm of the heaters were in the process of lifting from the surface as observed by Galloway and Mudawar. During the initial stages of lift off, a dark region would still exist in the photographs.

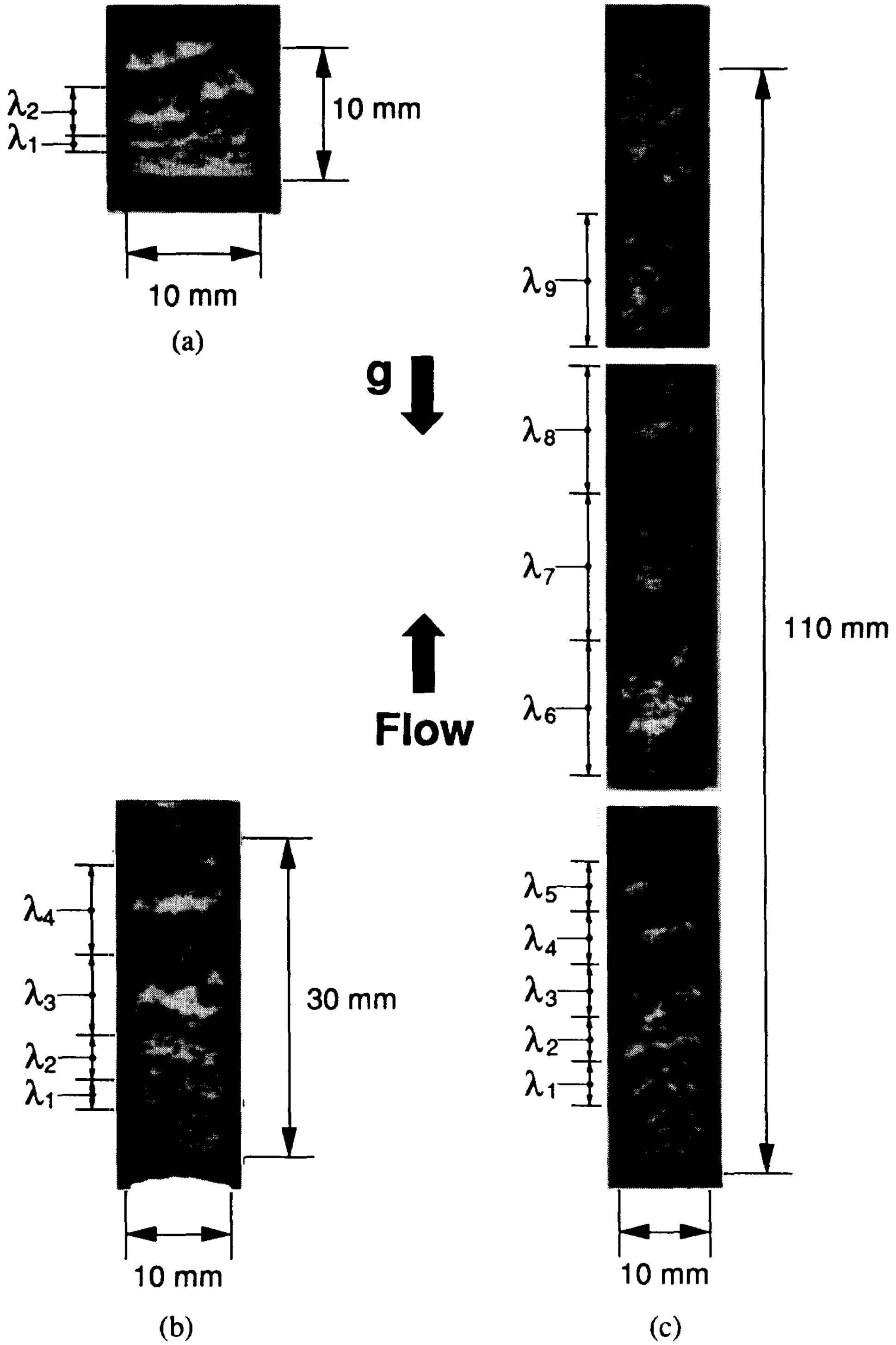

Fig. 5. Still photographs of the vapor–liquid interface on the (a) 10-mm, (b) 30-mm and (c) 110-mm heaters for an inlet velocity of 75 cm s^{-1} in vertical upflow.

Stream-wise growth of interfacial waves has been observed by several researchers in a variety of flow systems and conditions. Kirby *et al.* [18] observed bubbles periodically merged during fully-developed nucleate boiling on a heated tube. DeJarlais and Ishii [19] studied inverted annular flow by injecting liquid into a gas stream in the confines of a pipe. The liquid core broke through the gas stream and periodically touched the pipe wall for the first 250 mm before the phases became mixed. The distance between touch-down points grew with distance in the pipe. Andritsos and Hanratty [20] tested stratified air and water flow in a 25.2-mm pipe and observed large waves to coalesce, forming even larger and faster waves. Bui

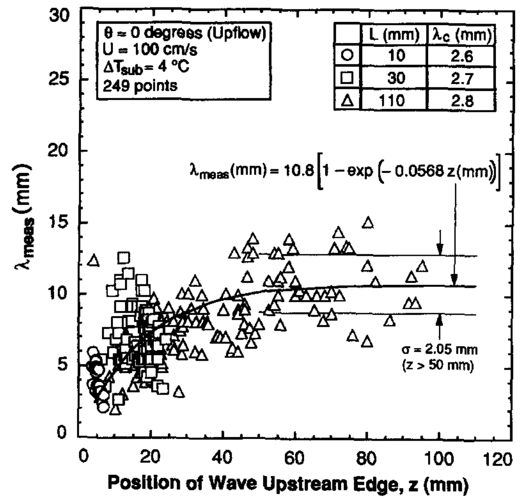

Fig. 6. Stream-wise variation of wavelength at CHF− for the three heaters at an inlet liquid velocity of 100 cm s^{-1}.

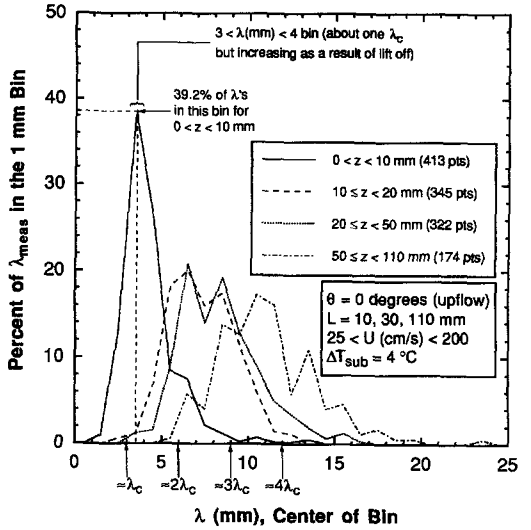

Fig. 7. Histogram of the measured wavelengths for all of the vertical upflow tests segregated by stream-wise position on the heaters.

and Dhir [21] saw vapor wave growth in a study of film boiling on a vertical plate in pool boiling. Although CHF had already occurred, they observed vapor bulges on the vapor film to feed vapor to each other. This increased the size of the recipient bulge at the donor's expense.

Three mechanisms of wave growth were identified by analyzing the video sequences of the present study and those of Galloway and Mudawar [9]. The growth in the wavelengths was found to be a combination of *wetting front lift off, wave stretching and drag-induced merging*; these processes are dealt with rigorously in the second part of this study [10]. Initially, interfacial wavelengths quickly doubled as postulated by Galloway and Mudawar. In the middle portion of the long heater, the interfacial wavelength increased by wave stretching and drag-induced wave merging, due to waves falling in the separation regions behind adjacent waves. In air-driven liquid wave experiments, Mudawar [22] found that certain waves would catch up and merge with preceding waves if the downstream wave was caught in the flow separation region behind the upstream wave.

Orientation effects

Figure 8(a)–(c) shows the 30-mm heater for $U = 50$ cm s^{-1} at the 0°, 45° and 90° orientations, respectively. Similar wave characteristics are visible for each orientation highlighting the small effect of orientation on the vapor waves. Again, wavelengths measured on the 10-mm heater and the first 10 mm of the 30-mm heater are similar for all of the orientations. At $\theta = 90°$, the vapor layer quickly filled the channel gap and reached the Lexan cover during the lower velocity tests with the 110-mm heater. Once this occurred, the distance between wetting fronts could no longer be accurately measured. Figure 9 displays all of the wave measurements made on all three heaters and three orientations for $U = 100$ cm s^{-1}. The negligible effect of orientation on λ_{meas} depicted in this figure is proof that the vapor velocity increases so rapidly that the Kelvin–Helmholtz instability becomes much more dominant than the Taylor instability in characterizing interfacial features even in horizontal flow.

Heater length effects

Figure 10 summarizes the observations of the liquid–vapor interface on the 110-mm heater. The distance between wetting fronts grew in the stream-wise direction decreasing the number of wetting fronts available for liquid replenishment of the heated surface. On the first few millimeters of each heater, the wavelength was approximately equal to the critical wavelength determined by the Kelvin–Helmholtz instability based on local conditions. On the 10-mm heater and the first 20 mm of the long heaters, zone L_1 in Fig. 10, the interfacial wavelength quickly increased to $2\lambda_c$. In the following 30 mm, zone L_2, the interfacial wavelength continued to increase, albeit with a little more spread in the data. Eventually, the wavelength on the 110-mm heater assumed a constant asymptotic value of approximately four times the critical wavelength, zone L_3 in Fig. 10. With a larger wavelength, fewer wetting fronts were available to dissipate the surface heat flux in the downstream regions as compared to the upstream region. This explains the observed increase in downstream thermocouple temperatures, Fig. 3(b), for the long heater at CHF− and the decrease in CHF with increasing heater length for all velocities and orientations, Fig. 4(a)–(c).

CHF trigger mechanism

The CHF trigger mechanism on the long heaters is the only remaining issue to be identified. Since the wetting front was formed upstream, its characteristics

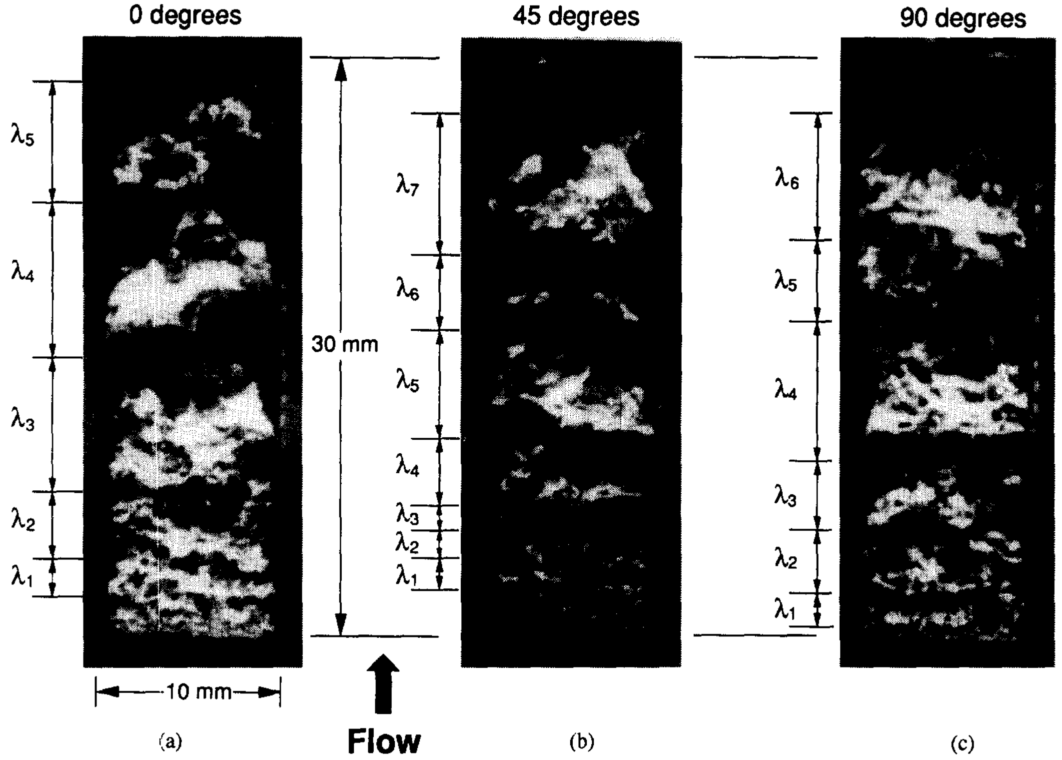

Fig. 8. Still photographs of the vapor–liquid interface on the 30-mm heaters for an inlet velocity of 50 cm s^{-1} at (a) 0°, (b) 45° and (c) 90° orientations.

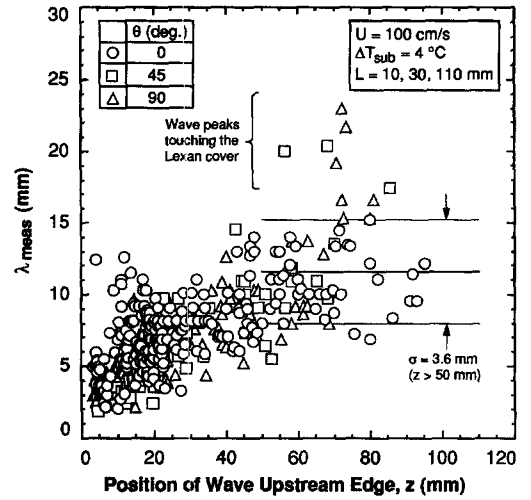

Fig. 9. Wavelengths measured on the three heaters at 0°, 45° and 90° orientations for an inlet velocity of 100 cm s^{-1}.

are assumed to be set at those local upstream conditions. As the vapor wave travels downstream and grows in length, there is no mechanism present to alter the size of the wetting front from its upstream length of $b \cdot (2\lambda_c)$, where b is the fraction of the vapor wavelength corresponding to interfacial contact with the heater surface. Therefore, the proper wetting front length of all the waves is $2b\lambda_c$, where b was observed to equal 0.25 [17]. Although the dark regions on the downstream wetting in Fig. 5(c) look bigger, this was a result of the flattening of the wavelength curvature and the increase in vapor volume in the wave. As the wavelength increases, more of the vapor wave resides close to the wall near the wetting front; thus this region looks darker. This is compounded by the increase in vapor volume and wave height which reflects more of the light from the flash while sheltering the wetting front region.

Lifting of the first wetting front, due to severe localized vapor effusion, was observed to be the catastrophic trigger for CHF on the long heaters as identified by Galloway and Mudawar [9] for short heaters. As the first wetting front lifts off, the heat flux becomes concentrated on a smaller number of downstream wetting fronts. Future wetting fronts cannot remain attached to the surface because of the local temperature rise. Since the vapor layer continues to move with a stream-wise velocity, the vapor sans the upstream wetting fronts quickly propagates downstream. The now higher heat fluxes in the remaining downstream wetting fronts promote even easier lift-off in those wetting fronts as well. The downstream propagation of the vapor blanket, coupled with the cessation of wetting front formation, is the trigger that precipitates CHF.

Figure 11 shows a 18 ms sequence of the CHF trigger mechanism on the 30-mm heater for $U = 100$ cm s^{-1} and $\theta = 0°$. Lifting of the most upstream wetting front at $t = 3$ ms can be seen propagating downstream over the next 15 ms leaving a continuous vapor blanket on the surface. As the vapor blanket moved

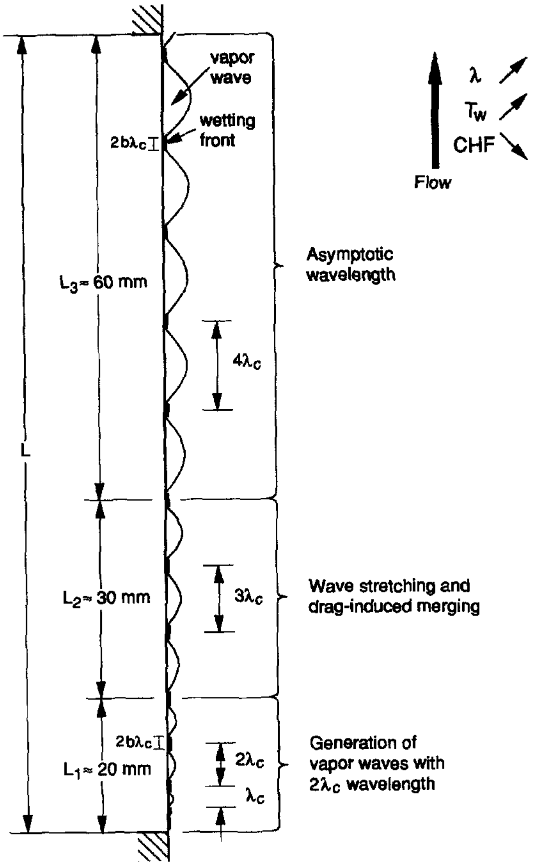

Fig. 10. Stream-wise reduction in CHF and increase in wall temperature with increased boiling length because of wavelength growth at CHF –.

downstream, wetting fronts can be observed to still exist on the downstream of the heater but not on the upstream, highlighting the notion that upstream lift-off is indeed the catastrophic trigger for CHF.

CONCLUSIONS

Observations were made of vapor–liquid interactions along 10-, 30- and 110-mm heaters in near-saturated flow of FC-72 and orientations ranging from vertical to horizontal in order to capture the effects of heater length and orientation on the trigger mechanism for CHF. The following conclusions may be drawn:

(1) A wavy vapor layer was observed to engulf the heater surface at CHF –, causing surface dryout except for discrete moving contact regions, wetting fronts, corresponding to the wave troughs. The distance between wetting fronts was observed to increase in the stream-wise direction from the initial Kelvin–Helmholtz critical wavelength value. Midway along the 110-mm heater, the waves reached an asymptotic value of four times the critical wavelength.

(2) As a result of the stream-wise growth of vapor wavelength, there was a decrease in the number of wetting fronts per unit length and, consequently, the downstream surface temperature increased at CHF – on the long heater. The stream-wise reduction in the number of wetting fronts also caused CHF to be highest for the 10-mm heater followed, in order, by the 30- and 110-mm heaters.

(3) Changes in orientation between vertical upflow

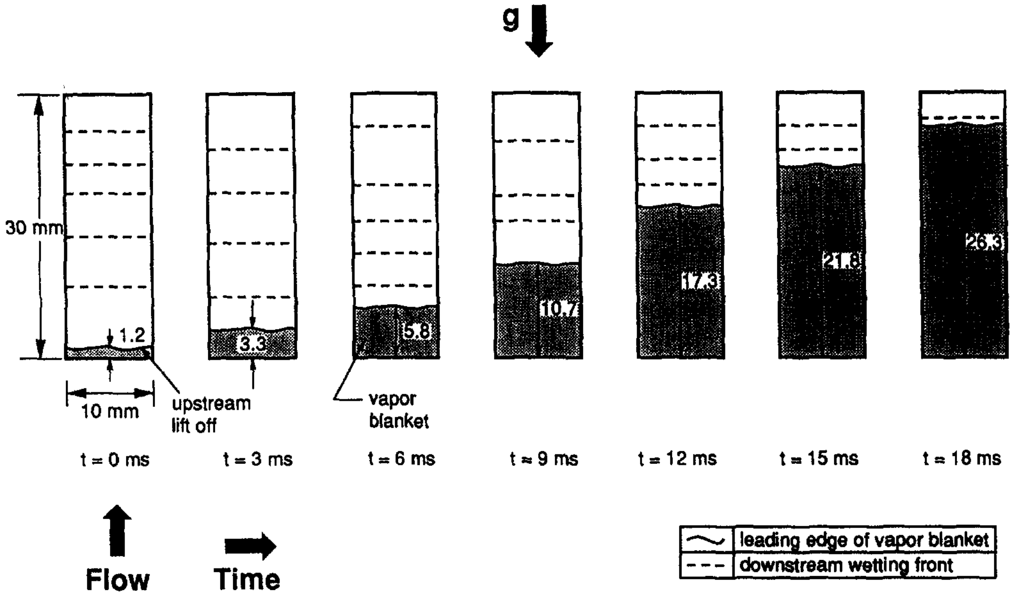

Fig. 11. Sequence of the catastrophic upstream wetting front lift off on the 30-mm heater for an inlet liquid velocity of 100 cm s^{-1} in vertical upflow.

and horizontal flow produced no appreciable effects on either the vapor wavelengths or the CHF values.

(4) Critical heat flux was triggered by lifting of the most upstream wetting front due to severe vapor effusion in the wetting front. This was followed by formation of a continuous vapor blanket at the upstream portion of the heater which advanced rapidly along the heater surface. The advancing vapor blanket caused a catastrophic cascading of downstream wetting front lift-off as heat flux in these wetting fronts increased, promoting even easier lift off, especially at the wetting front about to be taken over by the vapor blanket, where most of the heater upstream energy was channeled.

Acknowledgements—The authors gratefully acknowledge the support of the Office of Basic Energy Sciences of the U.S. Department of Energy (Grant No. DE-FG02-93ER14394). The authors also thank the Industrial Chemical Products Division of 3M Company for donating Fluorinert FC-72 for the present study.

REFERENCES

1. L. S. Tong and G. F. Hewitt, Overall viewpoint of flow boiling CHF mechanisms, ASME Paper 72-HT-54 (1972).
2. M. P. Fiori and A. E. Bergles, Model of critical heat flux in subcooled flow boiling, *Heat Transfer* 1970: *Proceedings of the Fourth International Heat Transfer Conference*, Paris, paper B6.3. Elsevier, Amsterdam (1970).
3. G. J. Kirby, R. Staniforth and J. H. Kinneir, A visual study of forced convection boiling—I. Results for a flat vertical heater, Report AEEW-R 281, United Kingdom Atomic Energy Authority Reactor Group (1965).
4. G. C. Vliet and G. Leppert, Critical heat flux for nearly saturated water flowing normal to a cylinder, *J. Heat Transfer Trans. ASME* **86,** 59–67 (1964).
5. G. C. Vliet and G. Leppert, Critical heat flux for subcooled water flowing normal to a cylinder, *J. Heat Transfer Trans. ASME* **86,** 68–74 (1964).
6. S. B. Van der Molen and F. W. B. M. Galjee, The boiling mechanism during burnout phenomena in subcooled two-phase water flows, *Heat Transfer* 1978: *Proceedings of the Sixth International Heat Transfer Conference*, Toronto, Vol. 1, pp. 381–385 (1978).
7. R. Hino and T. Ueda, Studies on heat transfer and flow characteristics in subcooled flow boiling—Part 1. Boiling characteristics, *Int. J. Multiphase Flow* **11,** 269–281 (1985).
8. R. Hino and T. Ueda, Studies on heat transfer and flow characteristics in subcooled flow boiling—Part 2. Flow characteristics, *Int. J. Multiphase Flow* **11,** 283–297 (1985).
9. J. E. Galloway and I. Mudawar, CHF mechanism in flow boiling from a short heated wall—I. Examination of near-wall conditions with the aid of photomicrography and high-speed video imaging, *Int. J. Heat Mass Transfer* **36,** 2511–2526 (1993).
10. C. O. Gersey and I. Mudawar, Effects of heater length and orientation on the trigger mechanism for near-saturated flow boiling critical heat flux—II. Critical heat flux model, *Int. J. Heat Mass Transfer* **38,** 643–654 (1995).
11. C. O. Gersey and I. Mudawar, Nucleate boiling and critical heat flux from protruded chip arrays during flow boiling, *J. Electron. Packag. Trans. ASME* **115,** 78–88 (1993).
12. C. O. Gersey and I. Mudawar, Orientation effects on the critical heat flux from discrete, in-line heat sources in a flow channel, *J. Heat Transfer Trans. ASME* **115,** 973–985 (1993).
13. C. O. Gersey and I. Mudawar, Effects of orientation on critical heat flux from chip arrays during flow boiling, *J. Electron. Packag. Trans. ASME* **114,** 290–299 (1992).
14. R. J. Moffat, Describing the uncertainties in experimental results, *Exp. Therm. Fluid Sci.* **1,** 3–17 (1988).
15. D. E. Maddox and I. Mudawar, Single and two-phase convective heat transfer from smooth and enhanced microelectronic heat sources in a rectangular channel, *J. Heat Transfer Trans. ASME* **111,** 1045–1052 (1989).
16. G. F. Hewitt and A. H. Govan, Phenomena and prediction in annular two-phase flow. In *Advances in Gas–Liquid Flows*—1990 (Edited by J. H. Kim, U. S. Rohatgi and A. Hashemi), Vol. HTD-155, pp. 41–56. ASME (1990).
17. J. E. Galloway and I. Mudawar, CHF mechanism in flow boiling from a short heated wall—II. Theoretical CHF model, *Int. J. Heat Mass Transfer* **36,** 2527–2540 (1993).
18. G. J. Kirby, R. Staniforth and J. H. Kinneir, A visual study of forced convection boiling—Part 2. Flow patterns and burnout for a round test section, Report AEEW-R 506, United Kingdom Atomic Energy Authority Reactor Group (1967).
19. G. DeJarlais and M. Ishii, Inverted annular flow experimental study, Report ANL-85-31, Argonne National Laboratory (1985).
20. N. Andritsos and T. J. Hanratty, Interfacial instabilities for horizontal gas–liquid flows in pipelines, *Int. J. Multiphase Flow* **13,** 583–603 (1987).
21. T. D. Bui and V. K. Dhir, Film boiling heat transfer on an isothermal vertical surface, *J. Heat Transfer Trans. ASME* **107,** 764–771 (1985).
22. I. Mudawar, Interfacial instabilities of air-driven liquid films, *Int. Commun. Heat Mass Transfer* **13,** 535–543 (1986).